

# Wideband Dual-Polarized Multiple Beam-Forming Antenna Arrays

He Zhu<sup>ID</sup>, Member, IEEE, Haihan Sun<sup>ID</sup>, Graduate Student Member, IEEE, Bevan Jones, Life Member, IEEE, Can Ding<sup>ID</sup>, Member, IEEE, and Y. Jay Guo<sup>ID</sup>, Fellow, IEEE

**Abstract**—Wideband multibeam antenna arrays based on three-beam Butler matrices are presented in this paper. The proposed beam-forming arrays are particularly suited to increasing the capacity of 4G long-term evolution (LTE) base stations. Although dual-polarized arrays are widely used in LTE base stations, analog beam-forming arrays have not been realized before, due to the huge challenge of achieving wide operating bandwidth and stable array patterns. To tackle these problems, for the first time, we present a novel wideband multiple beam-forming antenna array based on Butler matrices. The described beam-forming networks produce three beams but the methods are applicable to larger networks. The essential part of the beam-forming array is a wideband three-beam Butler matrix, which comprises quadrature couplers and fixed wideband phase shifters. Wideband quadrature and phase shifters are developed using striplines, which provide the required power levels and phase differences at the outputs. To achieve the correct beamwidth and to obtain the required level of crossover between adjacent beams, beam-forming networks consisting of augmented three-beam Butler matrices using power dividers are presented to expand the number of output ports from three to five or six. Dual-polarized, three-beam antenna arrays with five and six elements covering LTE band are developed. Prototypes comprising beam-forming networks and arrays are tested according to LTE base station specification. The test results show close agreement with the simulation ones and compliance with LTE requirements. The designs presented are applicable to a wide range of wideband multibeam arrays.

**Index Terms**—Antenna arrays, beam-forming networks, butler matrix, dual-linear polarization, long-term evolution (LTE) base stations, multibeam, phase shifters, quadrature couplers, wideband.

## I. INTRODUCTION

CROWDED data traffic is a major issue to tackle in the current wireless communication systems, especially in the 4G long-term evolution (LTE) base stations where high data rates are needed. Antenna features such as high gain, wide bandwidth, and high directivity are important and highly desired to meet the system requirements [1]–[4]. Linear arrays have been widely used in 2G, 3G, or LTE base stations to achieve these characteristics [5]–[10]. Dual-polarized antenna

Manuscript received August 9, 2018; revised October 9, 2018; accepted November 18, 2018. Date of publication December 19, 2018; date of current version March 5, 2019. This work was supported by the Australian Research Council (ARC) under Grant DP160102219. (*Corresponding author: He Zhu*)

The authors are with the Global Big Data Technologies Centre, University of Technology Sydney, Ultimo, NSW 2007, Australia (e-mail: he.zhu@uts.edu.au).

Color versions of one or more of the figures in this paper are available online at <http://ieeexplore.ieee.org>.

Digital Object Identifier 10.1109/TAP.2018.2888728

arrays consisting of four and eight elements achieved high gain of 14 and 16 dBi in [4] and [6], respectively. By interleaving high- and low-band elements, dual-band dual-polarized antenna arrays were designed in [6]–[9]. High gain and directivity were obtained in these and many similar arrays by employing vertical arrays (columns). In order to increase system capacity, base stations with multiple columns are widely used in MIMO configurations [11], [12].

Another way to increase capacity is using multiple beams to create more cells. In the areas of high traffic density such as concert arenas and sports stadiums, single-sector antennas may not provide sufficient capacity and it is desirable to divide the coverage area into a number of smaller cells served from a single point. In this case, antennas or antenna arrays with multiple beams covering multiple sectors can provide capacity advantages over single-sector antennas. Multibeam antennas that provide horizontally sectorized multiple-cell coverage within the areas for a particular event are of great interest. Another application of multibeam antennas is in the traditional three-sector cellular base stations where one or more of the sectors with high traffic density can be divided into subsectors with separate cells to increase capacity. In all these cases, a wideband analog beam-forming network serves as a key technology.

Typical beam-forming networks include Butler matrix, Blass matrix, and Nolen matrix, among which Butler matrix [13] is the most commonly used as it is simple and can be lossless in principle. Butler matrices have been employed in various smart antenna systems [14]–[17]. Most recently, there has been an increasing interest in Butler matrices, and various fabrication technologies such as low-temperature co-fired ceramic [18], waveguide [19], and substrate integrated waveguide [20]–[22] have been used to implement Butler matrices to millimeter-waves systems for 5G mobile or fixed wireless access communication. Various techniques for circuit miniaturization [23], [24], bandwidth enhancement [25], and beams control [26] have been applied to traditional  $4 \times 4$  Butler matrices, to obtain more attractive features. Traditional uniform Butler matrices usually include  $2^n$  input ports and  $2^n$  output ports, such as  $2 \times 2$ ,  $4 \times 4$ , and  $8 \times 8$  formats. In many cases, however,  $M \times N$  beam-forming networks are more desirable where the number of beams is not constrained to  $2^n$ . For cell sectorization, it is much more economical to choose the required number of beams based on the coverage requirements rather than needing to use  $2^n$  elements as adding extra cells is

costly if they are not needed. Some nonuniform beam-forming networks have been described such as in [27]–[29]; however, some of them are narrow-band solutions and none of them has been applied to wideband wireless communication systems-like LTE base stations.

In LTE base stations, arrays with multiple vertical columns of dual-polarization elements are arranged horizontally to achieve a narrow beam in the elevation direction and multiple beams in the azimuth direction, thereby meeting the need for large data capacity. Usually, a single beam antenna provides coverage over a  $120^\circ$  sector in the azimuth plane, whereas a multibeam antenna covers the same sector with multiple narrower beams corresponding to separate cells. In this case, the data capacity is dramatically increased due to the increased number of cells. For instance, a two-beam array integrated with a  $2 \times 4$  Butler matrix was described in [30] for covering one-sector of the traditional trisector base station to double the system capacity. However, though the beam number is doubled two beams may still not provide enough data capacity in some high-density areas. High-performance multibeam networks such as those presented here are essential for expanding the capacity of existing systems as population density increases, and single-beam antennas are a huge limitation in extending the data capacity of LTE systems. Therefore, there is an urgent industrial need to develop new solutions to build wideband multibeam arrays in wireless communication systems.

In this paper, we present the design of a wideband Butler matrix-based beam-forming network, which covers the LTE band from 1.71 to 2.69 GHz. The wideband beamforming network is employed in two alternative beam-forming arrays. The challenges are mainly from the requirements for wide operating bandwidth, pattern stability and sidelobe levels (SLLs), and in an environment of strong mutual coupling within arrays. Considering the existing shortcomings and challenges in the current LTE base stations, this paper has achieved the following contributions:

- 1) a wideband three-beam beam-forming network to cover the entire LTE band with flexible beamwidth;
- 2) new solutions for the design of key components in the beam-forming networks including wideband quadrature couplers, phase shifters, and power dividers;
- 3) dual-polarized antenna arrays using compact elements with stable patterns and steerable beams that meet LTE base station criteria;
- 4) excellent antenna array performance based on a reduced size element that minimizes coupling;
- 5) the beam-forming performance extends across the whole 4G band and has been verified by experiment.

This paper is organized as follows. Section II describes the configurations of beam-forming arrays to meet LTE base station criteria. Section III considers the theory of three-beam Butler matrix, based on which wideband components, including quadrature couplers and phase shifters are presented, modeled and simulated. Section IV gives thorough descriptions of wideband beam-forming networks that are used in LTE base stations to feed dual-polarized arrays. Section V presents the radiating element as well as arrays used in the multibeam arrays for validating the proposed beam-forming

networks. Section VI shows all the simulated and tested results of beam-forming arrays, confirming all the designs. Finally, Section VII concludes this paper.

## II. BEAM-FORMING NETWORKS FOR LTE BASE STATIONS

LTE base station antennas with multiple beams usually consist of beam-forming networks and an array of dual-linearly polarized antenna columns. In this paper, single elements are used in place of columns in order to study beam-forming in the azimuth plane. The beam-forming networks divide the coverage area in the azimuth plane into  $n$  (in our case three) parts. If the coverage sector is of angular width  $\alpha$ , then each beam should cover a sector of  $(\alpha/n)$ . In LTE base stations, three arrays are typically arranged to cover  $360^\circ$  arc and thus  $\alpha$  is  $120^\circ$  for each array. The crossover point is defined as the intersection point of two adjacent beams, which may have different levels relative to the beam peak depending on the array configurations. Basic Butler matrices are such that if the outputs are connected to omnidirectional elements, the beam crossovers occur at  $-3$  dB. For LTE multibeam antennas, the crossover level should normally be at about  $-10$  dB so, to achieve this, beams must be made narrower which can be achieved if the array is lengthened.

To this end, we extend the arrays from three elements to five or six elements as shown in Fig. 1, which shows block diagrams of the five- and six-element realizations. We refer to such a beam-forming network as an augmented Butler matrix. This achieves beam crossover values in the range from  $-10$  to  $-15$  dB, which is suitable for LTE applications. Here we intend to generate three beams in the azimuth plane to cover the  $120^\circ$  sector with three separate beams each covering a sector of  $40^\circ$ . Each beam-forming array is composed of two three-beam Butler matrices, power dividers/delay lines and a dual-linearly polarized array. Apart from its ability to control the crossover level between the beams, the augmented Butler matrix necessarily provides an amplitude taper across the array aperture which results in a reduced SLL. Some control of the SLL can be exercised by selecting the split ratio of the power dividers. A suitable arrangement of a five- and six-element beam-forming array is shown in Fig. 1. Tables I and II show the ideal power levels and phase distributions on the two arrays.

The three-beam Butler matrix is the essential part of the beam-forming network. To produce three beams, phase increments of  $0^\circ$ ,  $120^\circ$ , and  $-120^\circ$  are required between the outputs for the three required beams. These fixed phase relationships are required over the whole operating band. The Butler matrix is composed of quadrature couplers and fixed phase shifters. All of these components are required to be wideband devices. Fig. 2 shows how a three-way Butler matrix with the correct output amplitudes and phases can be constructed from quadrature couplers and fixed phase shifters. For each antenna element in the LTE base station,  $\pm 45^\circ$  polarization is required and separate beam-forming networks and dual-polarized radiating elements are needed for the two polarizations. In the cellular environment, the three inputs to

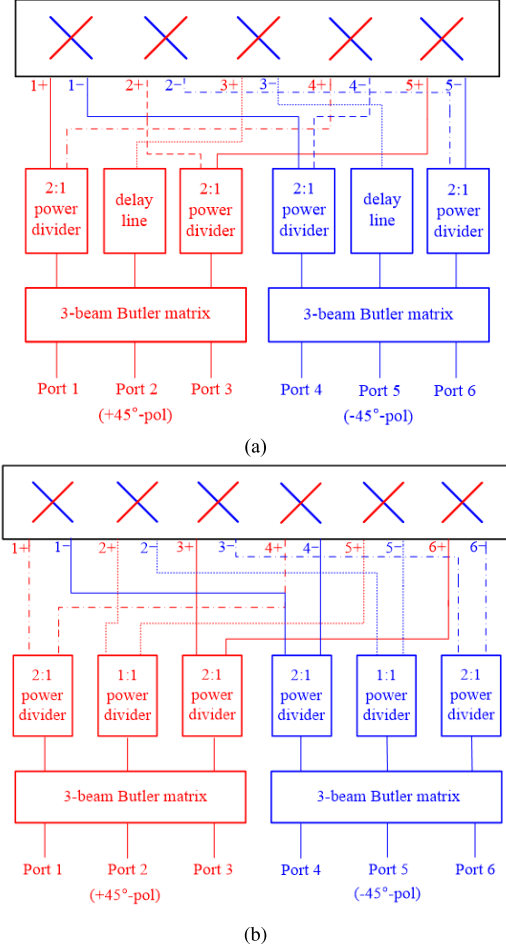


Fig. 1. Configurations of two beam-forming arrays for LTE base stations using (a) five-element array and (b) six-element array.

TABLE I  
POWER AND PHASE DISTRIBUTION ON THE FIVE-ELEMENT ARRAY

Element No.	1	2	3	4	5
Power Level	1/3	2/3	1	2/3	1/3
Amplitude (dB)	-4.77	-1.77	0	-1.77	-4.77

Element No.	1	2	3	4	5
Power Level	1/3	1/2	2/3	2/3	1/2
Amplitude (dB)	-4.77	-3	-1.77	-1.77	-3

TABLE II  
POWER AND PHASE DISTRIBUTION ON THE SIX-ELEMENT ARRAY

Element No.	1	2	3	4	5	6
Power Level	1/3	1/2	2/3	2/3	1/2	1/3
Amplitude (dB)	-4.77	-3	-1.77	-1.77	-3	-4.77

the Butler matrix correspond to three adjacent beams and are fed with signals for three separate cells. The single multibeam antenna is used as an alternative to three independent antennas with a different pointing fed from three separate cells.

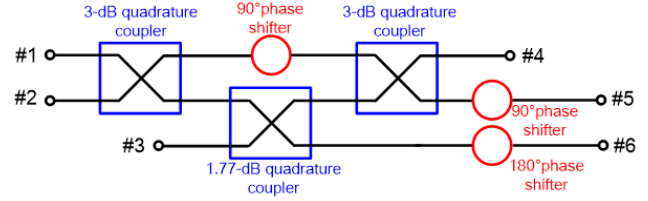


Fig. 2. Configuration of the proposed wideband three-beam Butler matrix for LTE base stations.

### III. DESIGN OF WIDEBAND THREE-BEAM BUTLER MATRIX

In this section, we provide the theory and engineering design of the essential components within the proposed wideband beam-forming network.

#### A. Theory of the Three-Beam Butler Matrix

For an ideal three-beam beam-forming network with perfect port matching and ideal isolation, the scattering matrix of the three-beam Butler matrix with ports 1, 2, and 3 as inputs and ports 4, 5, and 6 as outputs can be expressed as

$$S = \begin{bmatrix} 0 & T \\ T & 0 \end{bmatrix} \quad (1)$$

where

$$T = \frac{1}{\sqrt{3}} \begin{bmatrix} 1 & e^{j\frac{2\pi}{3}} & e^{-j\frac{2\pi}{3}} \\ 1 & e^{-j\frac{2\pi}{3}} & e^{j\frac{2\pi}{3}} \\ 1 & 1 & 1 \end{bmatrix}. \quad (2)$$

The matrix of the transmission block of  $S$  is a symmetrical unitary matrix. From (2), one can observe the phase differences between any two adjacent elements of each row (the former element minus the latter one) are  $-2\pi/3$ ,  $2\pi/3$ , and 0, respectively. To construct such a beam-forming network, quadrature couplers and fixed phase shifters are needed to provide appropriate power division and phase at each output port. The quadrature coupler can be represented with an orthogonal transmission matrix  $Q$ , which is written as

$$Q = \begin{bmatrix} a & j\sqrt{1-a^2} \\ j\sqrt{1-a^2} & a \end{bmatrix} \quad (3)$$

where  $a$  is the signal magnitude at one output port, and the signal magnitude at the other port is  $\sqrt{1-a^2}$ . There is  $90^\circ$  phase difference between two output ports due to the orthogonal property of the quadrature coupler. For the equal-split quadrature coupler  $Q_1$  with power division ratio (PDR) of 1:1 ( $a = 1/\sqrt{2}$ ) and unequal-split quadrature coupler  $Q_2$  with PDR of 2:1 ( $a = 1/\sqrt{3}$ ), the transmission matrices become, respectively

$$Q_1 = \begin{bmatrix} \frac{1}{\sqrt{2}} & j\frac{1}{\sqrt{2}} \\ j\frac{1}{\sqrt{2}} & \frac{1}{\sqrt{2}} \end{bmatrix} \quad (4a)$$

$$Q_2 = \begin{bmatrix} \frac{1}{\sqrt{3}} & j\frac{\sqrt{2}}{\sqrt{3}} \\ j\frac{\sqrt{2}}{\sqrt{3}} & \frac{1}{\sqrt{3}} \end{bmatrix}. \quad (4b)$$

The transmission block  $T$  can be written as

$$T = P_1 T_1 P_2 \quad (5)$$

where

$$T_1 = \begin{bmatrix} Q_1 & 1 \\ 1 & Q_2 \end{bmatrix} \begin{bmatrix} j & \\ & Q_1 & 1 \end{bmatrix} \quad (6a)$$

$$P_1 = \begin{bmatrix} e^{j\frac{\pi}{3}} & & \\ & e^{j\frac{\pi}{6}} & \\ & & 1 \end{bmatrix} \quad (6b)$$

$$P_2 = \begin{bmatrix} 1 & & \\ & j & \\ & & -1 \end{bmatrix}. \quad (6c)$$

Here,  $T_1$ ,  $P_1$ , and  $P_2$  are all diagonal matrices:  $T_1$  is the center part of  $T$  composed of three components: two equal-power quadrature couplers  $Q_1$  ( $a = 1/\sqrt{2}$ ) and one unequal-power quadrature coupler  $Q_2$  ( $a = 1/\sqrt{3}$ ) with a  $90^\circ$  phase shifter.  $P_1$  and  $P_2$  refer to two phase shifting networks, by which  $P_1$  will add phase shifts on the row elements while  $P_2$  will add phase shifts on the column elements of  $T_1$ .

In (2), the phases of the first elements of each row are identical. However, it makes no difference what this value is, which means the phase shift block  $P_1$  in (5) can be neglected, and the transmission block  $T$  of an ideal three-beam Butler matrix can be simplified to  $T_r$  as

$$T_r = T_1 P_2 = \frac{1}{\sqrt{3}} \begin{bmatrix} e^{j\frac{2\pi}{3}} & e^{j\frac{4\pi}{3}} & 1 \\ e^{j\frac{5\pi}{6}} & e^{j\frac{\pi}{6}} & e^{j-\frac{\pi}{2}} \\ e^{-j\pi} & e^{-j\pi} & e^{-j\pi} \end{bmatrix}. \quad (7)$$

It is seen that the phase differences between adjacent elements in each row are  $-2\pi/3$ ,  $2\pi/3$ , and 0, respectively, which satisfy the phase requirements of a three-beam Butler matrix. Based on the analysis above, the three-beam Butler matrix can be configured as shown in Fig. 2. The configuration is quite simple as it is composed of two 3 dB and one 1.77 dB quadrature couplers, and three phase shifters with  $90^\circ$  and  $180^\circ$  phase shifts. Since the design is aimed at LTE band range from 1.71 to 2.69 GHz, wideband components operating over this band need to be developed accordingly.

### B. Quadrature Couplers

Following the analysis above, we aim to develop a new type of quadrature couplers that can realize equal and unequal coupling power ratio with wide operating band range. To satisfy the requirements of the bandwidth and power ratio, directional couplers with coupled-lines using striplines are investigated. Fig. 3(a) shows the configuration of a traditional backward wave directional coupler with four ports. The overall length of the coupler is  $90^\circ$  at the center frequency, and the coupling factor of the coupled-line section is  $c$ . As mentioned in Section III-A, the output amplitude at two ports is  $a$  and  $\sqrt{1-a^2}$ , and  $a$  can be denoted as the coupling coefficient  $c$  in a coupler. If we write  $c = \sin \alpha$ , the scattering matrix of the coupler  $S_{c1}$  becomes [31]

$$S_{c1} = \begin{bmatrix} 0 & \cos \alpha & j \sin \alpha & 0 \\ \cos \alpha & 0 & 0 & j \sin \alpha \\ j \sin \alpha & 0 & 0 & \cos \alpha \\ 0 & j \sin \alpha & \cos \alpha & 0 \end{bmatrix} \quad (8)$$

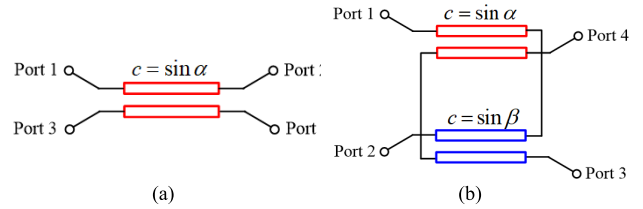


Fig. 3. Equivalent transmission line models of two quadrature couplers. (a) Traditional type. (b) Tandem type.

where  $\alpha$  is an angle depending on the PDR of the coupler. For a 3 dB coupler when the PDR equals to 1:1,  $\cos \alpha = \sin \alpha = 1/\sqrt{2}$  and  $\alpha = 45^\circ$ ; for a 1.77 dB coupler when the PDR equals to 2:1,  $\cos \alpha = 1/\sqrt{3}$ ,  $\sin \alpha = \sqrt{2}/\sqrt{3}$  and  $\alpha = 54.74^\circ$ . Ports 2 and 3 refer to the direct port and coupled port, where there is  $90^\circ$  phase difference between them; hence the term “quadrature coupler.”

For an unequal directional coupler with a PDR of 2:1, the coupling factor is about 0.82, which is so high that it is difficult to realize using planar structures. To tackle the problem, a tandem structure shown in Fig. 3(b) is used. Assuming that the coupling factors of the two coupled-line sections are  $\alpha$  and  $\beta$ , the output signal magnitude in this case can be calculated as:

- 1) Port 2:  $\cos \alpha \cos \beta - \sin \alpha \sin \beta = \cos(\alpha + \beta)$ ;
- 2) Port 3:  $j \cos \alpha \sin \beta + j \sin \alpha \cos \beta = j \sin(\alpha + \beta)$ .

Therefore, the scattering matrix of the cascaded quadrature coupler  $S_{c2}$  can be written as

$$S_{c2} = \begin{bmatrix} 0 & \cos(\alpha + \beta) & j \sin(\alpha + \beta) & 0 \\ \cos(\alpha + \beta) & 0 & 0 & j \sin(\alpha + \beta) \\ j \sin(\alpha + \beta) & 0 & 0 & \cos(\alpha + \beta) \\ 0 & j \sin(\alpha + \beta) & \cos(\alpha + \beta) & 0 \end{bmatrix}. \quad (9)$$

If  $\alpha = \beta$ , the scattering matrix can be simplified as

$$S_{c2} = \begin{bmatrix} 0 & \cos 2\alpha & j \sin 2\alpha & 0 \\ \cos 2\alpha & 0 & 0 & j \sin 2\alpha \\ j \sin 2\alpha & 0 & 0 & \cos 2\alpha \\ 0 & j \sin 2\alpha & \cos 2\alpha & 0 \end{bmatrix}. \quad (10)$$

Compared (10) with (8), it is found that the two-stage cascaded structure is able to realize a coupling factor that is twice that of the single stage coupler for the same degree of coupling of the lines. The even- and odd-mode impedances can be calculated by the following equations:

$$Z_{0e} = Z_0 \sqrt{\frac{1+c}{1-c}} \quad (11)$$

$$Z_{0o} = Z_0 \sqrt{\frac{1-c}{1+c}}. \quad (12)$$

In the cascaded structure, the coupling factor of the coupled-line is half that of the overall coupler. Therefore, for the 3 dB coupler, the even- and odd-mode impedances are 74.8 and 33.4  $\Omega$ ; for the 1.77 dB coupler, the even- and odd-mode impedances are 82.2 and 30.4  $\Omega$ , respectively. All ports of the quadrature couplers should be matched at all frequencies, requiring that the even and odd mode velocities are equal across the band. Microstrip construction has unequal velocities

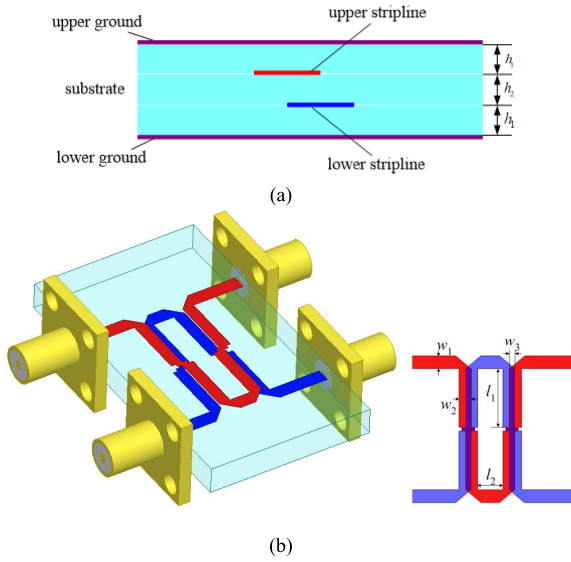


Fig. 4. Configuration of (a) cross-sectional view of the stripline implementation used in the design of quadrature coupler and (b) 3-D model of the constructed quadrature coupler.

TABLE III  
RELATED PARAMETERS OF TWO QUADRATURE COUPLERS

3-dB coupler		1.77-dB coupler	
Parameters	Values (mm)	Parameters	Values (mm)
$l_1$	9.2	$l_1$	8.8
$l_2$	3.0	$l_2$	3.0
$w_1$	1.96	$w_1$	1.96
$w_2$	1.5	$w_2$	1.52
$w_3$	0.24	$w_3$	0.76

and can only be approximately compensated [32]. Stripline inherently has equal even and odd mode velocities and normally provides much better performance where coupled lines are required. Fig. 4(a) shows the cross-sectional view of the proposed stripline, which has three stacked substrate boards each with dielectric constant of  $\epsilon_r$  and thickness of  $h_1$ ,  $h_2$ , and  $h_1$ , respectively. There are metal layers on the top and bottom of the substrates acting as grounds. Broadside coupling occurs between the upper and lower striplines, which are located on two sides of the middle substrate.

Fig. 4(b) shows the 3-D structure of the quadrature coupler. In this paper, two different couplers with coupling coefficient of 3 and 1.77 dB are built in Ansys EM Desktop (version 17.2), and the relevant dimensions of two couplers are listed in Table III. The coupling coefficient can be controlled by changing the linewidth as well as the overlap between the upper and lower stripline. The substrate used for the design is Rogers RO4356B with  $\epsilon_r$  of 3.48 and  $h_1$ ,  $h_2$  equal to 1.52 and 0.76 mm, respectively.

Full-wave simulation results are shown in Fig. 5. Fig. 5(a) shows that the power magnitude at port 2 and port 3 of two quadrature couplers with PDR of 1:1 and 2:1. For the equal PDR case,  $|S_{21}|$  and  $|S_{31}|$  is about  $-3.1 \pm 0.3$  dB across the frequency range from 1.7 to 2.7 GHz compared with the ideal power level  $-3$  dB. For the unequal coupler,  $|S_{21}|$  and  $|S_{31}|$  is about  $-1.9 \pm 0.2$  and  $-4.7 \pm 0.3$  dB, which is very

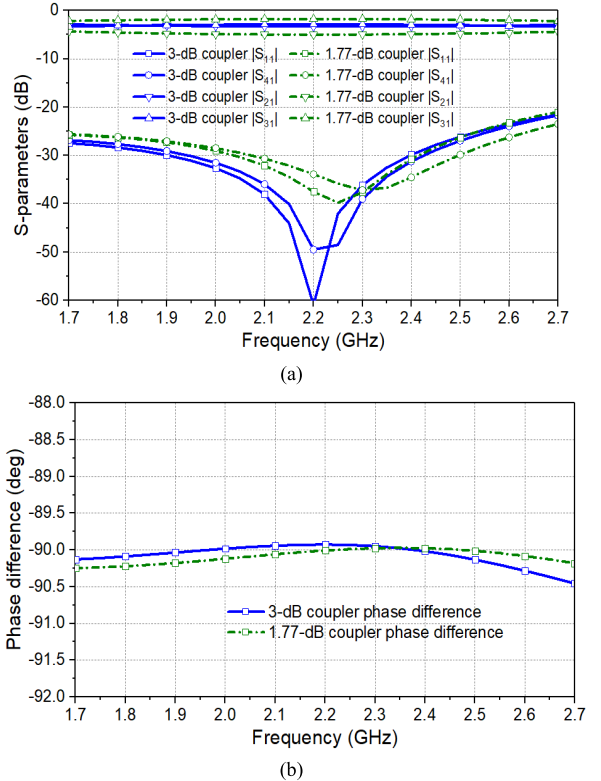


Fig. 5. Full-wave simulation results of the 3-dB and 1.77-dB quadrature couplers. (a) S-parameters. (b) Phase difference.

close to the ideal value of  $-1.77$  and  $-4.77$  dB. Fig. 5(b) demonstrates that both designs achieve excellent port matching and isolation across the whole band. Moreover, the phase difference between two output ports is constant and stable around  $90^\circ$ , representing the orthogonality property of the quadrature couplers.

### C. Wideband Fixed Phase Shifters

In addition to wideband quadrature couplers, fixed phase shifters are also critical components in the Butler matrix. To achieve stable phase, excellent matching and transmission property and small phase deviation are extremely important. To that end, a novel type of wideband phase shifter is designed. Fig. 6(a) shows the equivalent circuit of a suitable phase shifter. It comprises two transmission lines ( $Z_1, \theta_1$ ) and an open-ended stub ( $Z_2, \theta_2$ ) at the center point of two transmission lines. A reference line, as shown in Fig. 6(b), is required for comparison with the phase shifter section. The operating principle of the phase shifter is that if the inputs of the phase shifter and reference line (port 1 and port 3 in Fig. 6) are fed with equal, in-phase signals, the outputs maintain an almost constant phase difference across the band. The ABCD matrix of the phase shifter can be calculated by

$$[A] = \begin{bmatrix} \cos \theta_1 & j Z_1 \sin \theta_1 \\ j \frac{1}{Z_1} \sin \theta_1 & \cos \theta_1 \end{bmatrix} \cdot \begin{bmatrix} 1 & 0 \\ j \frac{1}{Z_2} \tan \theta_2 & 1 \end{bmatrix} \cdot \begin{bmatrix} \cos \theta_1 & j Z_1 \sin \theta_1 \\ j \frac{1}{Z_1} \sin \theta_1 & \cos \theta_1 \end{bmatrix}. \quad (13)$$

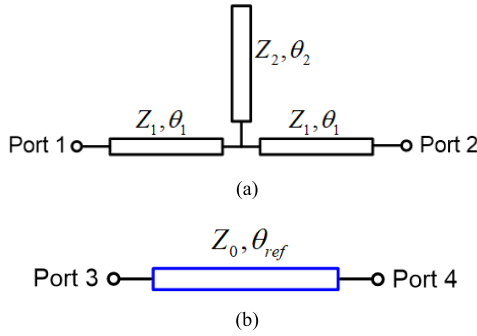


Fig. 6. Equivalent transmission line models of the wideband phase shifter. (a) Phase shifter. (b) Reference line.

Subsequently, using the ABCD-to-S-matrix conversion, the S-parameters of the phase shifter are derived as

$$S_{11} = \frac{B - CZ_o^2}{2Z_oA + B + CZ_o^2} \quad (14a)$$

$$S_{21} = \frac{2Z_o}{2Z_oA + B + CZ_o^2} \quad (14b)$$

where

$$\begin{aligned} A &= \cos(2\theta_1) - \frac{Z_1}{2Z_2} \sin(2\theta_1) \cdot \tan \theta_2 \\ B &= j \cdot \left[ Z_1 \sin(2\theta_1) - \frac{Z_1^2}{Z_2} \sin^2 \theta_1 \cdot \tan \theta_2 \right] \\ C &= j \cdot \left[ \frac{1}{Z_1} \sin(2\theta_1) - \frac{1}{Z_2} \cos^2 \theta_1 \cdot \tan \theta_2 \right]. \end{aligned}$$

The differential phase shift can be calculated by comparing the phase of the proposed structure with that of the reference line, which is expressed as

$$\begin{aligned} \Delta\phi &= \angle S_{21\_ps} - \angle S_{21\_ref} \\ &= \theta_r - \tan^{-1} \left[ \frac{B + CZ_o^2}{2j \cdot Z_o A} \right]. \end{aligned} \quad (15)$$

For an ideal wideband phase shifter, it is required to have  $|S_{21}| = 1$ ,  $|S_{11}| = 0$ , and  $\Delta\phi = \theta_r - 180^\circ$ . In this case, the related value can be determined as:  $\theta_1 = 90^\circ$  and  $\theta_2 = 180^\circ$ . These phase shifters can achieve a wide and constant differential phase across the desired operating band. To obtain  $90^\circ$  phase shift, the length of the reference line should be selected as  $\theta_r = 270^\circ$ . The impedance of  $Z_1$  and  $Z_2$  will affect the return loss, insertion loss and phase deviation within the operating band range. In this design, to cover the wideband range and keep a minimized phase deviation,  $Z_1$  and  $Z_2$  are selected as 30 and  $33 \Omega$ , respectively. To verify the design, full-wave simulation is done using the stripline structure. Fig. 7 shows the 3-D configuration of the phase shifter. It is noted that only one layer of stripline is used, which means the distances between the metal conductor and two grounds are different as  $h_1$  and  $h_1 + h_2$ , respectively.

Fig. 8 shows the comparison between the synthesized and full-wave simulation results of the structure. The full-wave simulation is done in the EM environment Ansys EM Desktop using the same substrate configuration as for the quadrature couplers. The optimized dimensions of the phase shifter are

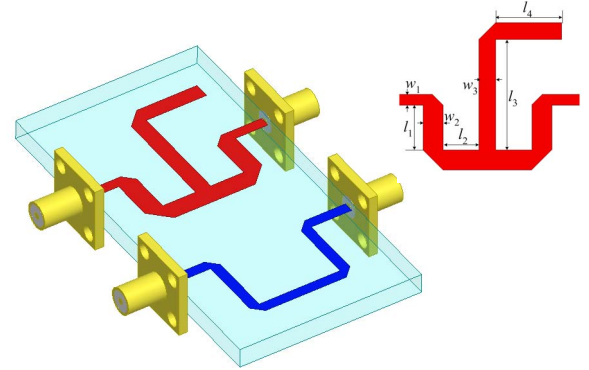


Fig. 7. 3-D model of the constructed phase shifter.

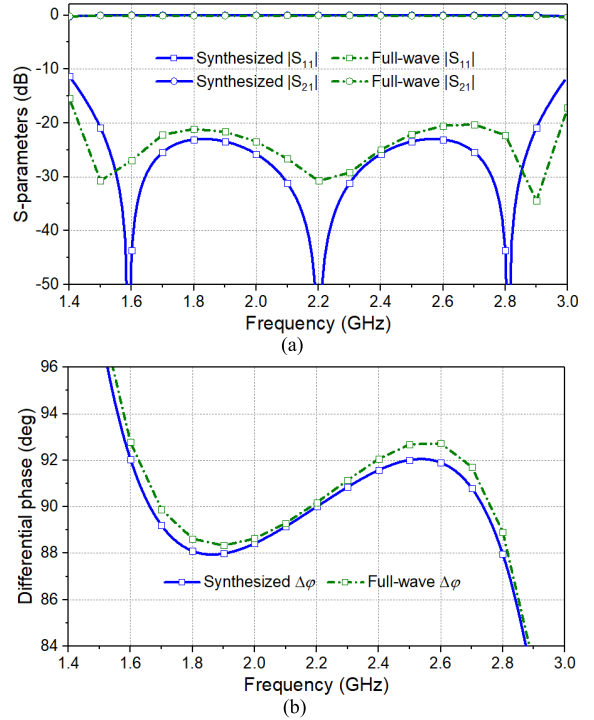


Fig. 8. Synthesized and full-wave simulation results of the phase shifter. (a) S-parameters. (b) Differential phase.

found to be:  $l_1 = 4.9$ ,  $l_2 = 5.14$ ,  $l_3 = 20$ ,  $l_4 = 13.9$ ,  $w_1 = 1.96$ ,  $w_2 = 3.6$ , and  $w_3 = 1.4$ , all in mm. The full-wave simulated result demonstrates that over the 1.7–2.7 GHz band, the return loss is more than 20 dB and insertion loss is close to 0 dB. Three resonant poles can be observed which greatly broaden the operating band. With regards to the differential phase,  $\Delta\phi$  is around  $90 \pm 2^\circ$  across the same band range, which makes it very suitable for minimizing the phase deviation of the beam-forming network. It is noted that another  $180^\circ$  phase shifter is also required in constructing the three-beam Butler matrix; however, since  $180^\circ$  requires extremely small value of impedance that is not practical to realize, it is feasible to use two  $90^\circ$  phase shift units to replace the  $180^\circ$  one in the following design process.

#### IV. WIDEBAND BEAM-FORMING NETWORKS

##### A. Modeling and Simulation of Butler Matrices

After the wideband quadrature couplers and phase shifters are designed, a three-beam Butler matrix can be created

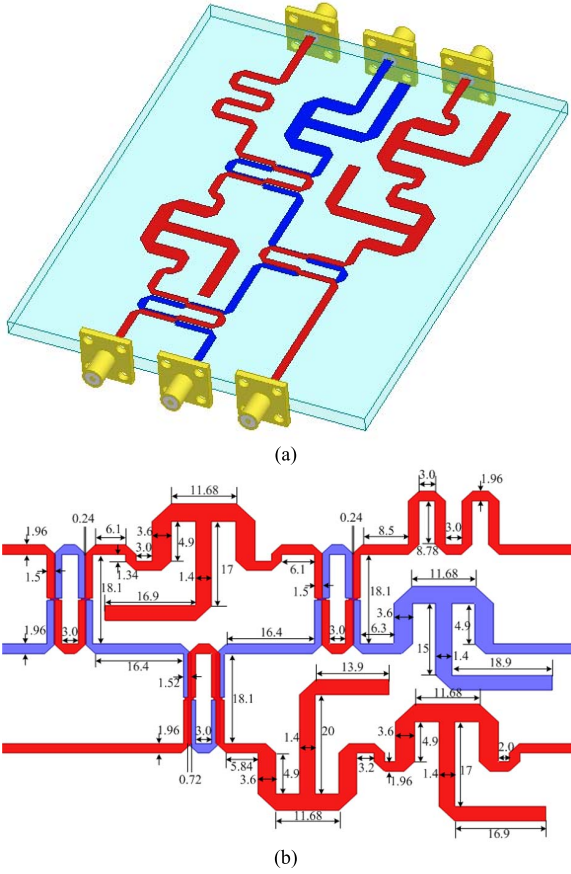


Fig. 9. Layout of the proposed three-beam Butler matrix for LTE base stations. (a) 3-D model. (b) 2-D layout with dimensions.

using the configuration shown in Fig. 2. Fig. 9(a) shows the 3-D model of the Butler matrix built in the full-wave environment Ansys EM Desktop. Stripline structure using the same substrate is used. To satisfy the requirement of differential phases at each port, appropriate length delay lines are implemented as meandered lines, making the structure more compact. Two 3 dB and one 1.77 dB quadrature couplers are used as indicated in the configuration of the beam-forming network shown in Fig. 2. Several 90° phase shifters provide 90° phase shift while two units are in series connection to provide 180° phase shift at port 6, which is in line with the configuration of the three-beam Butler matrix shown in Fig. 2. Specific dimensions of the structure are given in Fig. 9(b).

Fig. 10 shows the performance of the three-beam Butler matrix. As shown in Fig. 10(a), excellent matching at all ports and isolation between input ports is obtained with  $|S_{ii}|$  and  $|S_{ij}|(i, j = 1, 2, \text{ or } 3)$  are all less than  $-20$  dB across the band. The transmission from input to output terminals are given in Fig. 10(b), which are around  $-4.4$  to  $-5.8$  dB, and comparing well with the theoretical value of  $-4.77$  dB at each port, the overall insertion loss is around  $0.4$  dB. Fig. 10(c) shows the differential phase in all cases. To realize the multiple-beam antenna arrays, it is required to have differential phase of  $-120^\circ$ ,  $120^\circ$ , and  $0^\circ$ , respectively, when port 1, port 2, and port 3 are excited. The simulated phase deviation is

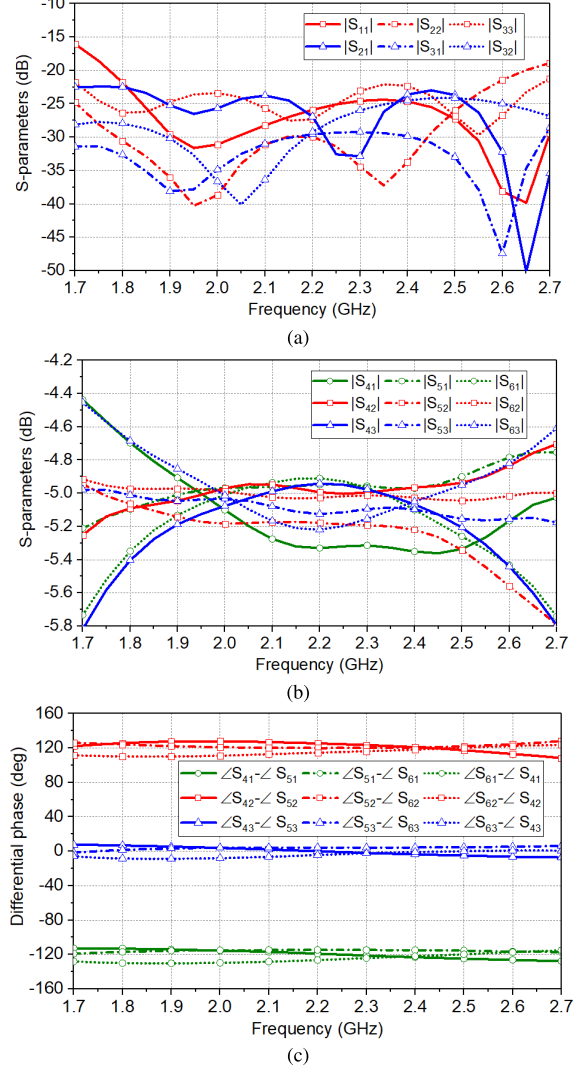


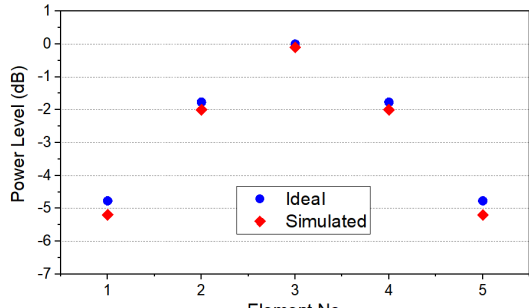
Fig. 10. Simulated S-parameters of the fabricated Butler matrix. (a) Return loss and isolations. (b) Transmission coefficients. (c) Differential phases.

around  $\pm 10^\circ$ . These results guarantee good matching, equal power, and constant phase increments for the beam-forming networks.

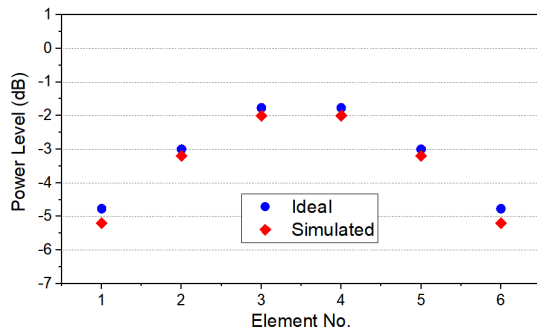
### B. Wideband Power Dividers

To build the beam-forming networks shown in Fig. 1, equal and unequal power dividers with equal phase outputs are needed. The power distributions of the five- and six-element arrays are tapered as shown in Fig. 11(a) and (b). This type of tapered distribution is applied in both cases and has the effect of reducing the SLLs [33]. For the five-element array, the center element has the highest power level of  $0$  dB and it decreases to  $-1.8$  and  $-4.8$  dB at the two edges. For the six-element array, the center two elements have the highest power level of  $-1.8$  dB, while the power levels at the other four elements are at  $-3$ ,  $-3$ ,  $-4.8$ , and  $-4.8$  dB, respectively.

Fig. 12 shows the configuration of the dividers and their equivalent circuit using ideal transmission lines. Due to the requirement for wide operating bandwidth, single-section

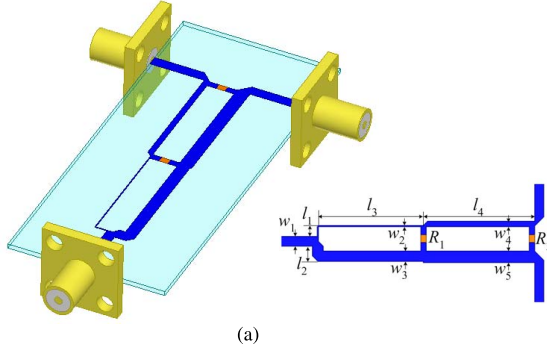


(a)

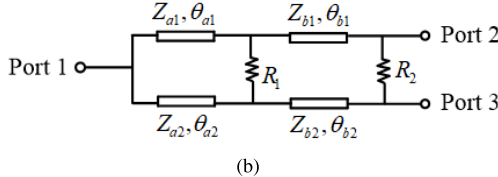


(b)

Fig. 11. Ideal and simulated power distribution for (a) five-element and (b) six-element beam-forming arrays.



(a)

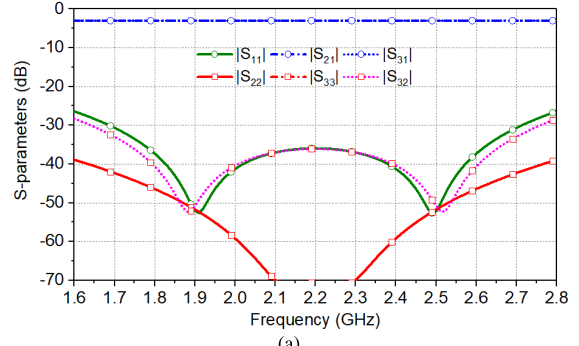


(b)

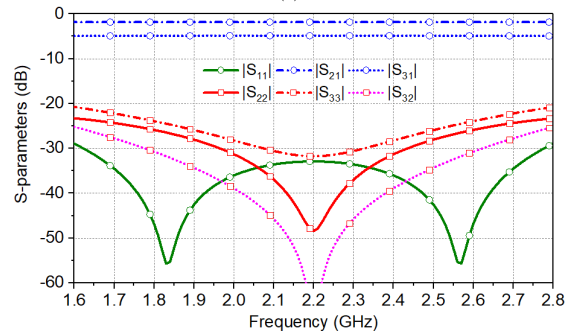
Fig. 12. Wideband Wilkinson dividers. (a) Printed circuit board realization. (b) Equivalent circuit.

Wilkinson power dividers are not suitable. Therefore, a two-section divider, composed of four transmission lines ( $Z_{a1}, \theta_{a1}$ ), ( $Z_{a2}, \theta_{a2}$ ), ( $Z_{b1}, \theta_{b1}$ ), and ( $Z_{b2}, \theta_{b2}$ ) and two isolation resistors ( $R_1, R_2$ ), is used, as indicated in Fig. 12(b). For wideband performance, the electrical length of each transmission line should be a quarter-wavelength at the center frequency. For an unequal power divider, we require  $S_{11} = S_{22} = S_{33} = S_{32} = 0$  and the amplitude ratio of outputs is  $|S_{21}|/|S_{31}| = k$ , and

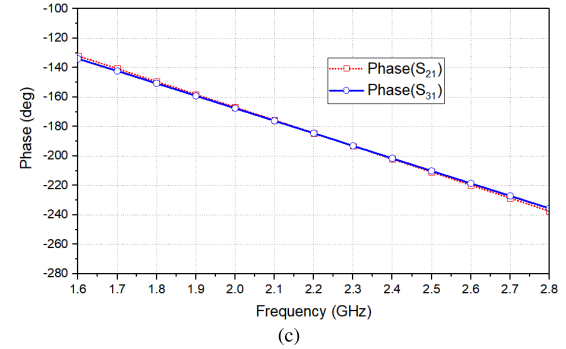
$$S_{21} = \frac{k}{\sqrt{k^2 + 1}} \quad (16)$$



(a)



(b)



(c)

Fig. 13. Simulated (a) magnitude of  $S_{11}$  and  $S_{21}$ , (b) magnitude of  $S_{31}$  and  $S_{41}$ , and (c) phases of  $S_{21}$  and  $S_{31}$  of the wideband power divider.

TABLE IV  
RELATED PARAMETERS OF TWO POWER DIVIDERS

Parameters	1:1 power divider		2:1 power divider	
	Values (mm)	Parameters	Values (mm)	Parameters
$l_1$	1.9	$l_1$	2.05	
$l_2$	1.9	$l_2$	2.85	
$l_3$	19.2	$l_3$	19.46	
$l_4$	20.1	$l_4$	20.56	
$w_1$	1.7	$w_1$	1.7	
$w_2$	0.69	$w_2$	0.15	
$w_3$	0.69	$w_3$	1.94	
$w_4$	1.33	$w_4$	0.94	
$w_5$	1.33	$w_5$	2.17	
$R_1$	100 $\Omega$	$R_1$	100 $\Omega$	
$R_2$	200 $\Omega$	$R_2$	240 $\Omega$	

$$S_{31} = \frac{1}{\sqrt{k^2 + 1}} \quad (17)$$

where  $k$  represents the square root of PDR  $k^2$  at two output ports. Obviously, the total output power should be equal to

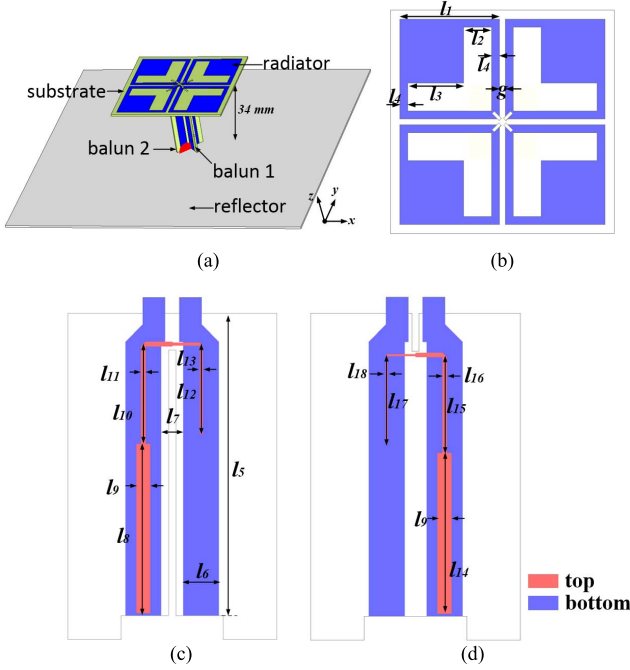


Fig. 14. Configuration of (a)  $\pm 45^\circ$ -polarized antenna element, (b) radiator, (c) balun 1, and (d) balun 2.

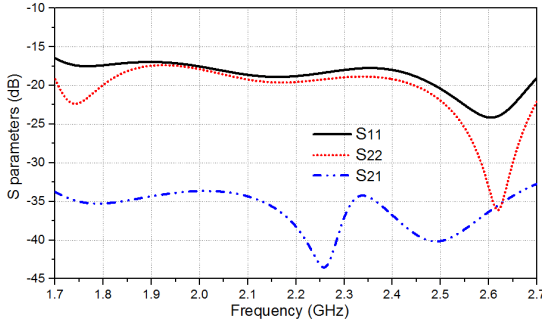


Fig. 15. Simulated S-parameters of the  $\pm 45^\circ$  -polarized single antenna element.

the input power. To obtain symmetrical power level distributions on the upper and lower lines, the following equation should be satisfied so as to avoid dissipation of power in \$R\_1\$ and \$R\_2\$:

$$k^2 = \frac{Z_{b1}}{Z_{a1}} = \frac{Z_{b2}}{Z_{a2}}. \quad (18)$$

Meanwhile, a suitable selection of isolation resistors \$R\_1\$ and \$R\_2\$ are given by

$$R_1 = 2Z_0 \quad (19)$$

$$R_2 = \left( k^2 + \frac{1}{k^2} \right) Z_0. \quad (20)$$

Here, two power dividers are needed—one with equal power division (\$k^2 = 1/1\$) and one with unequal division (\$k^2 = 2/1\$). Based on the analysis above, the S-parameters of two power dividers can be synthesized as given in Fig. 13(a) and (b). For the equal power divider, it is found that \$|S\_{21}| = |S\_{31}| = -3\$ dB and \$|S\_{11}|\$, \$|S\_{22}|\$, \$|S\_{33}|\$, and \$|S\_{23}|\$ are all below -25 dB. For the unequal case, \$|S\_{21}|\$ and \$|S\_{31}|\$ are -1.8 and -4.8 dB,

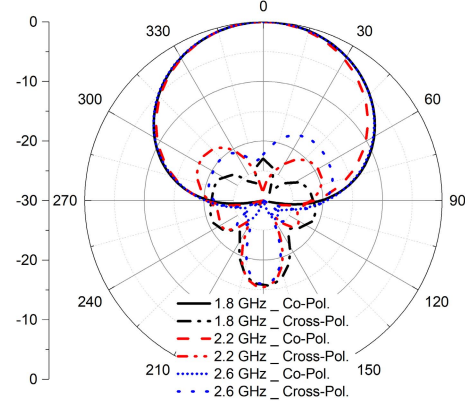


Fig. 16. Simulated radiation pattern at 1.8, 2.2, and 2.6 GHz for the  $\pm 45^\circ$ - polarized antenna element.

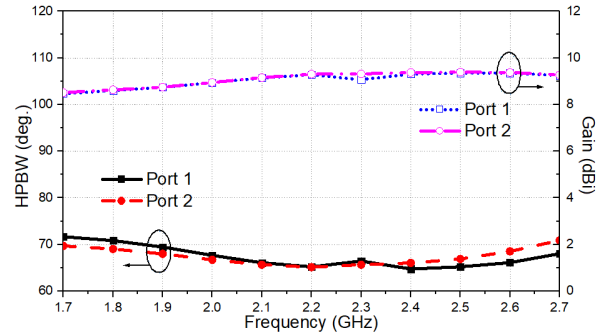


Fig. 17. Simulated HPBW and gain for the  $\pm 45^\circ$ -polarized antenna element.

TABLE V  
OPTIMIZED PARAMETERS OF THE  $\pm 45^\circ$ -POLARIZED ANTENNA ELEMENT

Parameters	Values (mm)	Parameters	Values (mm)
\$l_1\$	25	\$l_2\$	7
\$l_3\$	14	\$l_4\$	2
\$l_5\$	34	\$l_6\$	4
\$l_7\$	2.5	\$l_8\$	19
\$l_9\$	1.55	\$l_{10}\$	11.25
\$l_{11}\$	0.5	\$l_{12}\$	10.15
\$l_{13}\$	0.3	\$l_{14}\$	18
\$l_{15}\$	11	\$l_{16}\$	0.45
\$l_{17}\$	10	\$l_{18}\$	0.2
\$g\$	1.4		

respectively, with a difference of 3 dB indicating the power division of 2:1. The return loss at all ports and the isolation are greater than 20 dB across a wideband. The phase response of the unequal power divider is shown in Fig. 13(c). It is observed that the phase difference between two paths is smaller than  $\pm 1^\circ$  across the whole band, which can be regarded as an in-phase power divider. An EM structure is built, and the related dimensions are listed in Table IV. The simulated results agree well with the predicted ones, indicating that the design can provide proper power levels at outputs of the beam-forming networks and small reflections across such wideband range, which guarantee the overall performance of whole beam-forming network when integrated in systems.

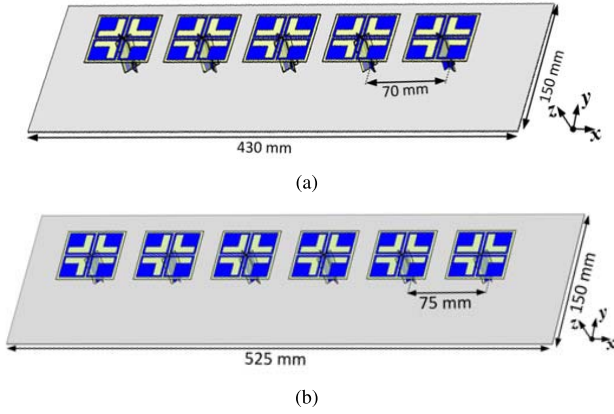


Fig. 18. Configuration of (a) five-element antenna array and (b) six-element antenna array.



Fig. 19. Photograph of the fabricated Butler matrix prototype.

## V. RADIATING ELEMENTS AND ARRAYS

This section shows the design of the radiating element and arrays used in the beam-forming arrays. To obtain stable patterns and minimize the effect of mutual coupling between elements, a compact structure of dual-polarized element is proposed and verified. Simulations have been conducted on a single isolated radiating element as well as on the beam-forming arrays.

### A. Configuration of the Radiating Element

The configuration of the  $\pm 45^\circ$ -polarized antenna element is shown in Fig. 14. The reason for this selection is the small size of the element which permits a half-wavelength spacing. This should minimize the mutual coupling between elements. Each element consists of a square-shaped cross-dipole, two perpendicular baluns, and a flat square ground reflector. For each dipole arm, a square metal piece is added in the square loop for convenient matching and minimizing the radiator's size. The cross-dipole is printed on the top of a substrate of dielectric constant 4.3 and thickness 1.0 mm. Two baluns are designed to excite the cross-dipole to achieve  $\pm 45^\circ$  polarizations. The detailed design procedure with impedance matching for the wideband balun was presented in [34] and is not repeated here. The optimized dimensions of the element are listed in Table V. The element features a compact size of  $51.4 \times 51.4 \text{ mm}^2$ .

The simulated S-parameters for a single isolated element are shown in Fig. 15. The antenna elements at both polarizations are well-matched with  $|S_{11}|$  and  $|S_{22}|$  below  $-16.5 \text{ dB}$  across

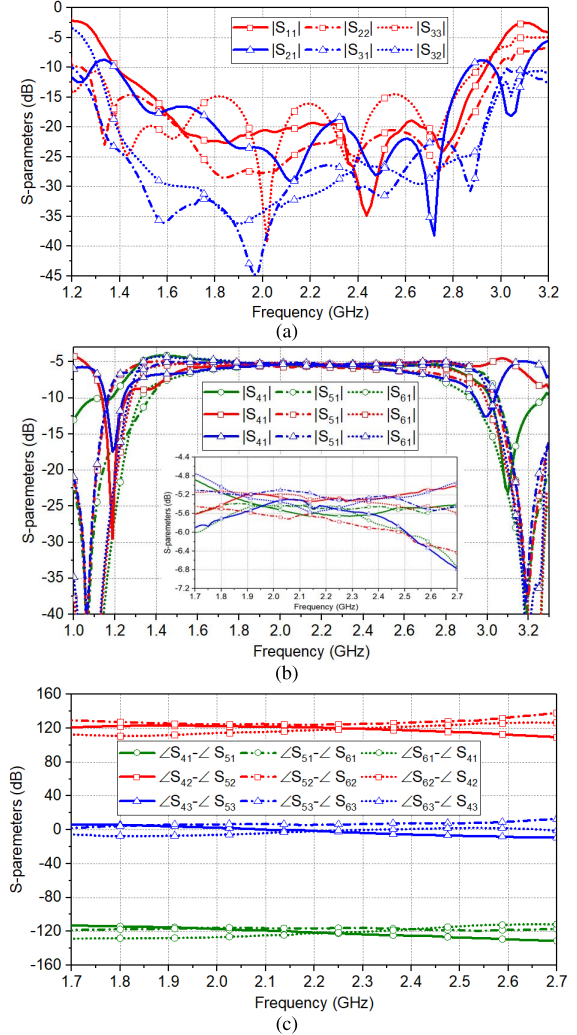


Fig. 20. Measured S-parameters of the fabricated Butler matrix. (a) Return loss and isolations. (b) Transmission coefficients. (c) Differential phases.

the band. The coupling between the two polarizations is less than  $-33 \text{ dB}$  across the band. The radiation pattern of the element for one polarization at 1.8, 2.2, and 2.6 GHz is given in Fig. 16, from which very stable radiation patterns can be observed, with cross-polarization level less than  $-22 \text{ dB}$  at boresight. The simulated horizontal HPBW and gain performance are shown in Fig. 17, which shows that the HPBW varies within  $68^\circ \pm 2^\circ$  and the gain fluctuates around  $9.0 \text{ dBi}$  from 1.7 to 2.7 GHz for the two polarizations. The good performance of the antenna element contributes to reliable pattern of antenna arrays used in the beam-forming arrays. While the elements were designed in isolation, the performance of the array is calculated in the presence of mutual coupling.

### B. Arrays

Two arrays are designed as shown in Fig. 18. The spacing between the elements is of critical importance for the SLL and grating lobe level (GLL) for beams offset from boresight. The small size of the elements provides the freedom for the array arrangement. The spacing between the elements is important in arrays. For the five-element and six-element arrays, the distances are set to be 70 mm ( $\sim 0.50\lambda_0$ ) and 75 mm

TABLE VI  
OVERALL PERFORMANCE OF THE SIX-ELEMENT ARRAY FED BY THE BEAM-FORMING NETWORK

	1.8 GHz			2.2 GHz			2.6 GHz		
	Port 1	Port 2	Port 3	Port 1	Port 2	Port 3	Port 1	Port 2	Port 3
Beam angle	-42°	42°	0°	-36°	36°	0°	-30°	30°	0°
HPBW	23°	23°	20°	20°	20°	16°	16°	16°	13°
Realized Gain (dBi)	12	11.8	13	13	13.2	14.8	14.8	14.6	15.1
Cross-pol Level (dB)	-22	-16	-15	-18	-19	-15	-11	-14	-22
Side-lobe Level (dB)	-13	-14	-14	-13	-13	-15	-15	-14	-17

TABLE VII  
COMPARISON BETWEEN THIS PAPER WITH OTHER BEAM-FORMING NETWORKS AND ANTENNA ARRAYS

Ref.	Type	Configuration	FR (GHz)	BW (%)	IL (dB)	RL (dB)	Isolation (dB)	Antenna Realization	Gain (dBi)	HPBW (°)
[15]	4 × 4	Microstrip	5.8-6.4	9.8	NG	-10	-18	Yes	8.7-9.8	NG
[16]	8 × 8	Stripline	2.45	NA	2-3	-10	NG	Yes	7.4-10.8	NG
[17]	4 × 4	Microstrip	4.4-5.8	23.5	NG	-12	NG	Yes	~7.1	36
[19]	4 × 8	Waveguide	58.5-62.5	4	NG	-10	-10	Yes	25-27	17-21
[20]	4 × 4	SIW	25-28	11.3	1.5-3	-10	NG	Yes	11.9-12.8	NG
[21]	4 × 4	SIW	8.5-10.6	22	NG	-15	-15	No	NA	NA
[23]	4 × 4	Microstrip	1	NA	1.75	-18	-15	No	NA	NA
[24]	4 × 4	Microstrip	0.96-1.04	8	1.5	-10	-10	Yes	NG	NG
[25]	4 × 4	Three-layer Microstrip	1.96-3.15	47	1.4-3.4	-15	NG	Yes	NG	NG
[26]	4 × 4	Microstrip	2.4	NA	1.7	-14	-18.2	Yes	7-10	26-42.5
[27]	3 × 3	Microstrip	5.6-6	7	1-2.4	-15	-20	Yes	~10	NG
[28]	3 × 4	Microstrip	2.1-3	37	1.5-3	-15	-15	No	NA	NA
[29]	3 × 3	Microstrip	1.7-2.7	46	1-4	-14	-20	No	NA	NA
[30]	2 × 8	Microstrip	1.7-2.2 2.4-2.8	26 15.4	NG	-15	-10	Yes	7.2-8.5	58-60 80-84
This work	3 × 5 3 × 6	Stripline	1.7-2.7	46	0.5-1.5	-15	-18	Yes	11.8-15.1	16-20

\* FR: frequency range; BW: bandwidth; IL: insertion loss; RL: return loss; HPBW: half-power beamwidth; NG: not given; NA: not applicable.

( $\sim 0.54\lambda_0$ ), respectively. These are optimized to minimize the SLL and GLL across the band. The antenna arrays are fed from two sets of beam-forming networks for the two polarizations.

## VI. EXPERIMENTAL RESULTS AND DISCUSSION

### A. Experimental Results of the Three-Beam Butler Matrix

Finally, a prototype of beam-forming network as well as the beam-forming array are built and tested for validation. Fig. 19 shows the fabricated prototype of the wideband three-beam Butler matrix. Since the design is implemented in stripline technology, the top and bottom layer are ground while the tracks are in the central layers and are not visible. Its overall performance is shown in Fig. 20. The measured results agree well with the predictions. As observed from Fig. 20(a), within the band, all return loss values from input ports and isolation values between any two input ports ( $|S_{ii}|$  and  $|S_{ij}|$ ,  $i, j = 1, 2$ , or  $3$ ) are greater than 15 dB. The transmission properties of  $|S_{ji}|$  ( $i = 1, 2$ , or  $3$ , and  $j = 4, 5$ , or  $6$ )

are  $-5.8 \pm 1.0$  dB, which means the insertion loss is around 1.0 dB for all signals. The tested differential phases at all ports are  $-120^\circ$ ,  $120^\circ$ , and  $0^\circ$  when port 1, port 2, and port 3 are excited with around  $\pm 10^\circ$  deviation, which is the same as the simulation. These results guarantee that the three beams of the multibeam arrays are preserved across the LTE band.

### B. Experimental Results of Beam-Forming Arrays

The test environment and the overall structure of the beam-forming arrays are shown in Fig. 21(a) and (b). The three-beam Butler matrix is cascaded with the three power dividers using adapters, and then the output ports of power dividers are connected with six array elements using cables. Since the two beam-forming arrays in Fig. 11 are similar in terms of structure and testing procedure, only the case of  $+45^\circ$  pol of the six-element array is given here. It is noted that due to the limitations of the test equipment, we rotated the array by  $90^\circ$  and tested the pattern in the elevation plane.

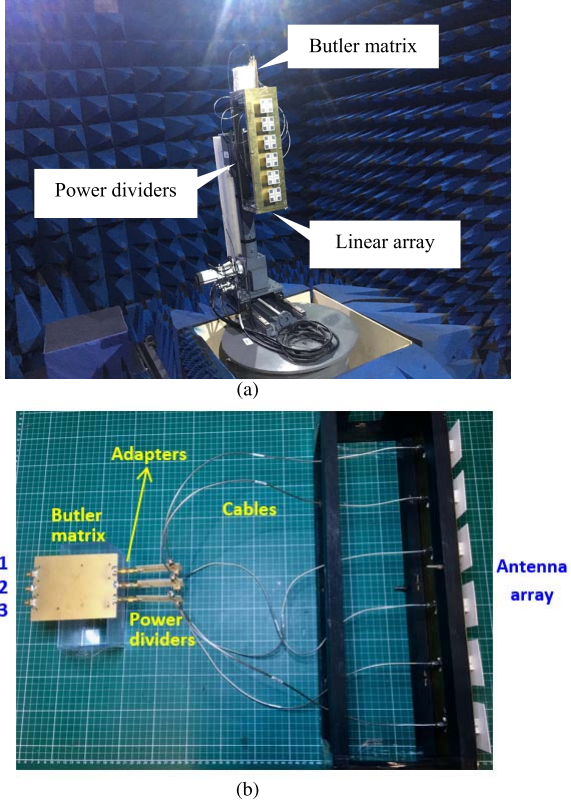


Fig. 21. Tested LTE beam-forming array including the beam-forming network and six-element antenna array. (a) Test environment. (b) Overall structure.

Fig. 22 shows the measured return losses ( $|S_{11}|$ ,  $|S_{22}|$ , and  $|S_{33}|$ ) and isolation ( $|S_{21}|$ ,  $|S_{31}|$ , and  $|S_{32}|$ ) of the two beam-forming arrays comprising the beam-forming networks and antenna arrays. In both systems with five-element or six-element arrays, good matching with return loss greater than 12.2 dB is achieved across the band from 1.6 to 2.8 GHz. Some reflections are caused by the cables, adapters and connectors used within the beam-forming arrays. Isolation better than 11 dB is obtained over the band. It is observed in Fig. 22 that more ripples are produced in the band compared with in Fig. 20(a) with only the Butler matrix. This phenomenon is due to the multiple reflections generated by the power dividers and antenna arrays.

The radiation patterns obtained from the six-element array fed by the beam-forming network are presented in Fig. 23. Three spaced beams beam 1, beam 2, and beam 3 are generated when port 1, port 2, and port 3 are excited, respectively. Since the beams obtained using the five-element and six-element arrays are similar, only the patterns of the six-element array are shown. The simulated and measured patterns are provided at three frequencies, 1.8, 2.2, and 2.6 GHz. Good agreement between the simulated patterns and the measured ones is achieved. Three contiguous beams with different pointing angles are realized by the beam-forming network across the LTE band. As shown in Fig. 23(a)–(c), beams at 1.8 GHz point at  $-42^\circ$ ,  $42^\circ$ , and  $0^\circ$  when port 1, port 2, and port 3 of the beam-forming network are excited, respectively. The measured horizontal HPBW of these three states are  $23^\circ$ ,  $23^\circ$ , and  $20^\circ$ , which are exactly those predicted. The realized

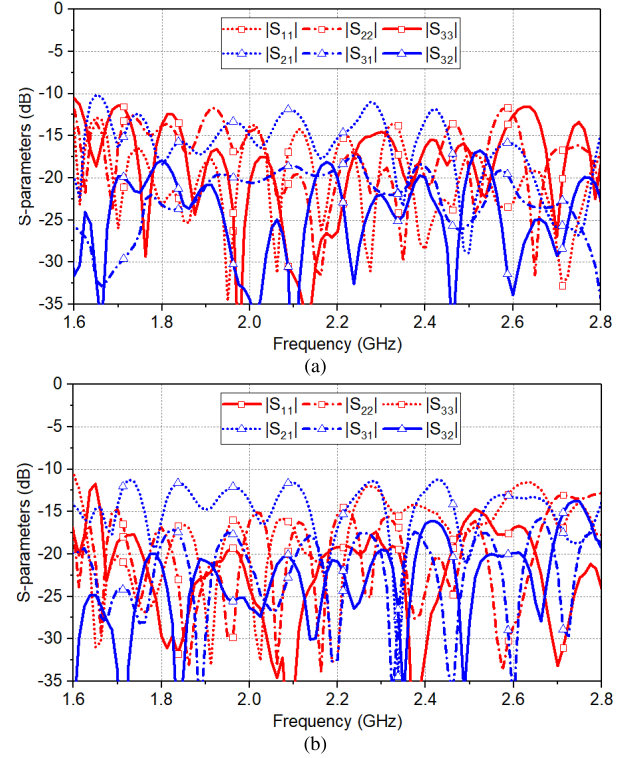


Fig. 22. Measured return loss and isolation at input ports of two beam-forming arrays using (a) five-element array and (b) six-element array.

gain is around 11.8–13 dBi and the SLL is below  $-12$  dB. At 2.2 GHz as shown in Fig. 23(d)–(f), the beam point at  $-36^\circ$ ,  $36^\circ$ , and  $0^\circ$  and HPBWs are around  $20^\circ$ ,  $20^\circ$ , and  $16^\circ$  when port 1, port 2, and port 3 are excited. The realized measured gain is around 12.6–13.8 dBi, compared with the simulated value of 13–14.8 dBi. The SLL is below  $-13$  dB and cross-polarization level less than  $-15$  dB at the center of each beam. Fig. 23(g)–(i) displays the radiation patterns at 2.6 GHz with three beams pointing to  $-30^\circ$ ,  $30^\circ$ , and  $0^\circ$ , respectively. The HPBW is around  $16^\circ$ ,  $16^\circ$ , and  $13^\circ$ , and realized gain is 13.5–14.6 dBi. The SLL is below  $-17$  dB and cross-polarization level less than  $-16$  dB.

### C. Discussion

The overall performance of the beam-forming arrays is given in Table VI. As expected, as the operating frequency increases from 1.8 to 2.6 GHz, the beam-pointing angle slightly moves to the boresight, the HPBW becomes narrower, and the realized gain is slightly increased. The SLL is improved as the operating frequency increases, but a grating lobe rises. These effects are mainly due to the variation of the spacing in wavelengths between elements. The variation of the pattern across the band is not significant and the beam crossover level between adjacent beams is almost constant. The achieved crossover values for the five- and six-element arrays are  $-10$  and  $-15$  dB, which are exactly in line with the target. It is noted that the mutual coupling of the arrays has been included in all simulations. The patterns hardly change between 1.71 and 1.8 GHz as well as between 2.6 and 2.69 GHz.

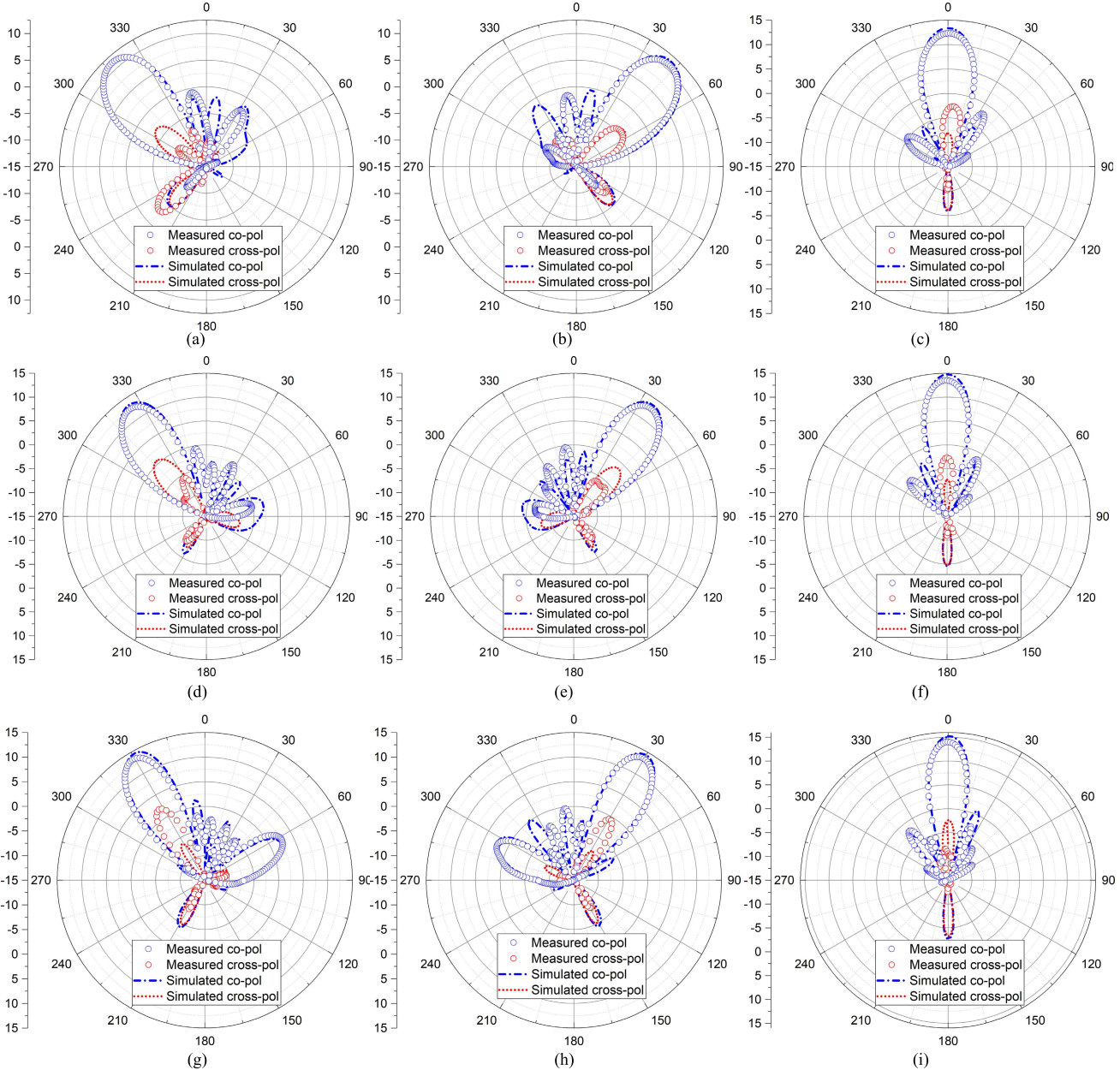


Fig. 23. Simulated and measured radiation patterns at 1.8, 2.2, and 2.6 GHz for the six-element antenna array fed by the beam-forming network. (a) Beam 1 at 1.8 GHz. (b) Beam 2 at 1.8 GHz. (c) Beam 3 at 1.8 GHz. (d) Beam 1 at 2.2 GHz. (e) Beam 2 at 2.2 GHz. (f) Beam 3 at 2.2 GHz. (g) Beam 1 at 2.6 GHz. (h) Beam 2 at 2.6 GHz. (i) Beam 3 at 2.6 GHz.

Table VII shows the comparison between the performance obtained in this paper and other beam-forming arrays. In Table VII, the overall performance of beam-forming networks (such as insertion loss, return loss, and isolation) and the performance of antenna arrays (including the realized gain and half-power beamwidth) are given. From the circuit perspective, the beam-forming network in this paper has excellent performance including the lowest loss, small reflection, high isolation across, and wide operating bandwidth. In order to get stable patterns, compact dual-polarized antenna arrays are developed using a compact antenna element. The antenna arrays are well matched by wideband baluns with the mutual coupling considered. The presented beam-forming network and beam-forming arrays have demonstrated the largest

operating bandwidth and the most stable patterns across the targeted LTE band range.

It is noted that the beam-forming network can generate three adjacent beams radiating at different angles to cover a certain area in the azimuth plane. Since the measured isolation between the beam-forming inputs is high, there is very little interference between these three beams. Therefore, signals targeted at different subsectorial regions can be transmitted at different ports of the beam-forming networks simultaneously. In this way, the function of transmitting multiple beams is realized and thus the data capacity of the communication system is tripled. It is also noted that in this paper, three-beam beam-forming networks are considered because of their importance in LTE networks. The same circuit techniques are

applicable to the more usual  $2^n$ -way networks where wideband operation is required. A four-way matrix implemented with these components will have similar loss, isolation and return loss performance.

## VII. CONCLUSION

In this paper, a novel wideband beam-forming network and two multiple beam-forming arrays for LTE base stations have been presented and verified. The designs are described in detail and are directly applicable to other configurations covering the LTE band. Thorough analysis of a beam-forming network generating three beams has been given. The design of wideband components including quadrature couplers, phase shifters, and power dividers are reported. Since the stripline techniques are used throughout the whole design, the overall loss of the circuit is extremely small. To implement the function of beam-forming network, two different LTE subsystem configurations are designed and verified with antenna arrays composed of five and six  $\pm 45^\circ$  dual-linearly polarized elements. Measurements have been conducted successfully on the beam-forming networks as well as on the two beam-forming arrays. The results show that the proposed design can increase system capacity by producing multiple beams in free space, which can be used in a wide range of multibeam LTE base stations.

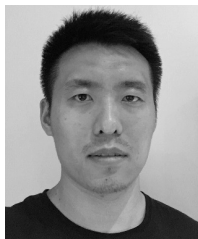
## ACKNOWLEDGMENT

The authors would like to thank Prof. J. Huang and F. Qiu at the School of Electronics Information and Electrical Engineering, Xiangnan University, Chenzhou, China, for their help with the testing of the beam-forming arrays.

## REFERENCES

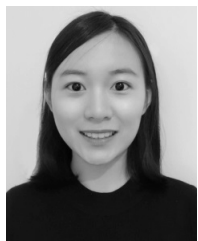
- [1] H. D. Chen, C. Y. D. Sim, J. Y. Wu, and T. W. Chiu, "Broadband high-gain microstrip array antennas for WiMAX base station," *IEEE Trans. Antennas Propag.*, vol. 60, no. 8, pp. 3977–3980, Aug. 2012.
- [2] C.-X. Mao, S. Gao, Y. Wang, F. Qin, and Q.-X. Chu, "Multimode resonator-fed dual-polarized antenna array with enhanced bandwidth and selectivity," *IEEE Trans. Antennas Propag.*, vol. 63, no. 12, pp. 5492–5499, Dec. 2015.
- [3] C.-X. Mao *et al.*, "An integrated filtering antenna array with high selectivity and harmonics suppression," *IEEE Trans. Microw. Theory Techn.*, vol. 64, no. 6, pp. 1798–1805, Jun. 2016.
- [4] C. Ding, H. Sun, R. W. Ziolkowski, and Y. J. Guo, "Simplified tightly-coupled cross-dipole arrangement for base station applications," *IEEE Access*, vol. 5, pp. 27491–27503, 2017.
- [5] H. Huang, Y. Liu, and S. Gong, "A broadband dual-polarized base station antenna with sturdy construction," *IEEE Antennas Wireless Propag. Lett.*, vol. 16, pp. 665–668, 2017.
- [6] Y. Cui, R. Li, and H. Fu, "A broadband dual-polarized planar antenna for 2G/3G/LTE base stations," *IEEE Trans. Antennas Propag.*, vol. 62, no. 9, pp. 4836–4840, Sep. 2014.
- [7] H. Huang, Y. Liu, and S. Gong, "A novel dual-broadband and dual-polarized antenna for 2G/3G/LTE base stations," *IEEE Trans. Antennas Propag.*, vol. 64, no. 9, pp. 4113–4118, Sep. 2016.
- [8] H. Huang, Y. Liu, and S. Gong, "A dual-broadband, dual-polarized base station antenna for 2G/3G/4G applications," *IEEE Antennas Wireless Propag. Lett.*, vol. 16, pp. 1111–1114, 2017.
- [9] Y. He, Z. Pan, X. Cheng, Y. He, J. Qiao, and M. M. Tentzeris, "A novel dual-band, dual-polarized, miniaturized and low-profile base station antenna," *IEEE Trans. Antennas Propag.*, vol. 63, no. 12, pp. 5399–5408, Dec. 2015.
- [10] Y. He, W. Tian, and L. Zhang, "A novel dual-broadband dual-polarized electrical downtilt base station antenna for 2G/3G applications," *IEEE Access*, vol. 5, pp. 15241–15249, 2017.
- [11] G. Li, H. Zhai, L. Li, C. Liang, R. Yu, and S. Liu, "AMC-loaded wideband base station antenna for indoor access point in MIMO system," *IEEE Trans. Antennas Propag.*, vol. 63, no. 2, pp. 525–533, Feb. 2015.
- [12] D. Manteuffel and R. Martens, "Compact multimode multielement antenna for indoor UWB massive MIMO," *IEEE Trans. Antennas Propag.*, vol. 64, no. 7, pp. 2689–2697, Jul. 2016.
- [13] J. Butler and R. Lowe, "Beam forming matrix simplifies design of electronically scanned antennas," *Electron. Des.*, vol. 9, pp. 170–173, Apr. 1961.
- [14] M. Elhefnawy and W. Ismail, "A microstrip antenna array for indoor wireless dynamic environments," *IEEE Trans. Antennas Propag.*, vol. 57, no. 12, pp. 3998–4002, Dec. 2009.
- [15] C. Liu, S. Xiao, Y.-X. Guo, M.-C. Tang, Y.-Y. Bai, and B. Z. Wang, "Circularly polarized beam-steering antenna array with Butler matrix network," *IEEE Antennas Wireless Propag. Lett.*, vol. 10, pp. 1278–1281, 2011.
- [16] C.-C. Chang, R.-H. Lee, and T.-Y. Shih, "Design of a beam switching/steering Butler matrix for phased array system," *IEEE Trans. Antennas Propag.*, vol. 58, no. 2, pp. 367–374, Feb. 2010.
- [17] C. Liu, S. Xiao, Y.-X. Guo, Y.-Y. Bai, and B.-Z. Wang, "Broadband circularly polarized beam-steering antenna array," *IEEE Trans. Antennas Propag.*, vol. 61, no. 3, pp. 1475–1479, Mar. 2013.
- [18] Y. J. Cheng, X. Y. Bao, and Y. X. Guo, "60-GHz LTCC miniaturized substrate integrated multibeam array antenna with multiple polarizations," *IEEE Trans. Antennas Propag.*, vol. 61, no. 12, pp. 5958–5967, Dec. 2013.
- [19] K. Tekkouk, J. Hirokawa, R. Sauleau, M. Ettorre, M. Sano, and M. Ando, "Dual-layer ridged waveguide slot array fed by a Butler matrix with sidelobe control in the 60-GHz band," *IEEE Trans. Antennas Propag.*, vol. 63, no. 9, pp. 3857–3867, Sep. 2015.
- [20] A. B. Guntupalli, T. Djerafi, and K. Wu, "Two-dimensional scanning antenna array driven by integrated waveguide phase shifter," *IEEE Trans. Antennas Propag.*, vol. 62, no. 3, pp. 1117–1124, Mar. 2014.
- [21] S. Karamzadeh, V. Rafii, M. Kartal, and B. S. Virdee, "Compact and broadband  $4 \times 4$  SIW Butler matrix with phase and magnitude error reduction," *IEEE Microw. Wireless Compon. Lett.*, vol. 25, no. 12, pp. 772–774, Dec. 2015.
- [22] J.-W. Lian, Y.-L. Ban, Q.-L. Yang, B. Fu, Z.-F. Yu, and L.-K. Sun, "Planar millimeter-wave 2-D beam-scanning multibeam array antenna fed by compact SIW beam-forming network," *IEEE Trans. Antennas Propag.*, vol. 66, no. 3, pp. 1299–1310, Mar. 2018.
- [23] Y. S. Jeong and T. W. Kim, "Design and analysis of swapped port coupler and its application in a miniaturized Butler matrix," *IEEE Trans. Microw. Theory Techn.*, vol. 58, no. 4, pp. 764–770, Apr. 2010.
- [24] E. Gandini, M. Ettorre, R. Sauleau, and A. Grbic, "A lumped-element unit cell for beam-forming networks and its application to a miniaturized Butler matrix," *IEEE Trans. Microw. Theory Techn.*, vol. 61, no. 4, pp. 1477–1487, Apr. 2013.
- [25] T.-H. Lin, S.-K. Hsu, and T.-L. Wu, "Bandwidth enhancement of  $4 \times 4$  Butler matrix using broadband forward-wave directional coupler and phase difference compensation," *IEEE Trans. Microw. Theory Techn.*, vol. 61, no. 12, pp. 4099–4109, Dec. 2013.
- [26] H. N. Chu and T.-G. Ma, "An extended  $4 \times 4$  Butler matrix with enhanced beam controllability and widened spatial coverage," *IEEE Trans. Microw. Theory Techn.*, vol. 66, no. 34, pp. 1301–1311, Mar. 2018.
- [27] K. Ding, X. Fang, Y. Wang, and A. Chen, "Printed dual-layer three-way directional coupler utilized as  $3 \times 3$  beamforming network for orthogonal three-beam antenna array," *IEEE Antennas Wireless Propag. Lett.*, vol. 13, pp. 911–914, 2014.
- [28] H. Nachouane, A. Najid, A. Tribak, and F. Riouch, "Wideband  $3 \times 4$  Butler matrix using Wilkinson divider for MIMO applications," in *Proc. Int. Conf. Next Gener. Netw. Services (NGNS)*, 2014, pp. 101–105.
- [29] J. P. Wang, S.-H. Hsu, and W.-J. Chen, "Two-Layer three-beam-generating matrix for broadband beamforming with microstrip," in *Proc. IEEE Int. Symp. Antennas Propag. (AP-S)*, Jul. 2017, p. 2347.
- [30] X.-Y. Zhang, D. Xue, L.-H. Ye, Y.-M. Pan, and Y. Zhang, "Compact dual-band dual-polarized interleaved two-beam array with stable radiation pattern based on filtering elements," *IEEE Trans. Antennas Propag.*, vol. 65, no. 9, pp. 4566–4575, Sep. 2017.
- [31] D. M. Pozar, *Microwave Engineering*, 2nd ed. Hoboken, NJ, USA: Wiley, 1997.
- [32] K. C. Gupta, R. Garg, I. Bahl, and P. Bhartia, *Microstrip Lines and Slotlines*, 2nd ed. Norwood, MA, USA: Artech House, 1996.

- [33] S. Gruszcynski, K. Wincza, and K. Sachse, "Reduced sidelobe four-beam  $N$ -element antenna arrays fed by  $4 \times N$  Butler matrices," *IEEE Antennas Wireless Propag. Lett.*, vol. 5, pp. 430–434, 2006.
- [34] H. Sun, C. Ding, B. Jones, and Y. J. Guo, "A wideband base station antenna element with stable radiation pattern and reduced beam squint," *IEEE Access*, vol. 5, pp. 23022–23031, 2017.



**He Zhu** (M'18) received the B.Sc. and M.Eng. degrees from the South China University of Technology, Guangzhou, China, and the Ph.D. degree in electrical engineering from the School of ITEE, University of Queensland, Brisbane, Australia.

He is currently a Post-Doctoral Research Fellow with the Global Big Data Technologies Centre, University of Technology Sydney, Sydney, Australia. His current research interests include the development of passive and tunable microwave and millimeter-wave devices, radio frequency integrated circuits and systems, and beam-forming networks for antenna arrays.



**Haihan Sun** (GS'17) was born in Shandong, China, in 1994. She received the bachelor's degree in electronic information engineering from the Beijing University of Posts and Telecommunications, Beijing, China, in 2015. She is currently pursuing the Ph.D. degree in engineering with the University of Technology Sydney, Sydney, Australia.

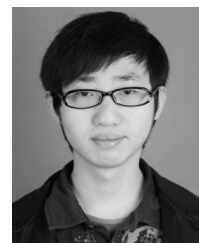
Her current research interests include base station antennas and wideband omnidirectional antennas.



**Bevan Jones** (LM'13) was born in Sydney, Australia. He received the B.Sc., B.E. (Hons.), and Ph.D. degrees in electrical engineering from the University of Sydney, Sydney, in 1967, 1970, and 1974, respectively.

From 1974 to 1977, he was a Post-Doctoral Fellow with the Max-Planck-Institut für Radioastronomie, Bonn, Germany, with a focus on the design of a millimeter wavelength radio telescope. He was a Lecturer with Wollongong University, Wollongong, Australia, for two years. He returned to Germany as a Scientist to continue his previous work. He returned to Australia in 1980 to work on the Interscan Project to develop a microwave aircraft landing system. From 1980 to 1982, he led a group of 12 Australian engineers working on this project in the USA with a joint venture partner. From 1983 to 1994, he was a Technical Director of Interscan Australia Pty Ltd, a research and development company owned and funded by the Australian Industry Development Corporation. He led the development of many antenna-based products including the microwave landing system, a C-band phased array precision approach system, an electronically scanned TACAN navigation beacon, a large vertical aperture secondary surveillance radar antenna, and an advanced S-band multibeam phased array primary radar antenna. From 1992 to 1993, he was responsible for the development of early cellular base station antennas, the first with adjustable electrical beam tilt at the time when the original AMPS system was being rolled out. In 1994, together with two partners, he founded Argus Technologies, Sydney, where he served as the Managing Director for ten years and then as the Technical Director. The company has specialized solely in the design and manufacture of cellular base station antennas and expanded its market reach worldwide. The company initially operated in Sydney but setup a second manufacturing facility in Guangzhou, China, in 2001 and later established a research and development capability there. Since its inception,

Argus has brought many innovations to market and became a major international supplier of cellular antennas. In 2011, the company was acquired by a USA multinational where he served as the Technical Director under the new ownership for a further two years, during which time he was largely engaged in technical instruction of the group's engineering teams in the USA and China. Following that, he retired from full-time work and since then has done a number of consulting jobs on antenna related topics. He has taught specialist courses in numerical methods and electromagnetics at universities. He has done consulting on antennas and electromagnetics for a number of companies including Raytheon and British Aerospace. He is currently an Adjunct Professor with the University of Technology Sydney, Sydney. He has authored or co-authored over a number of articles in technical journals and patents relating to antenna components.



**Can Ding** (M'17) was born in Anhui, China, in 1989. He received the bachelor's degree in microelectronics from Xidian University, Xi'an, China, in 2009, and the Ph.D. degree from Macquarie University, Sydney, Australia, in 2015.

From 2012 to 2015, he is under the Cotutelle agreement between Macquarie University and Xidian University. During this period, he is also with Commonwealth Scientific and Industrial Research Organization DPAS Flagship, Marsfield, Australia. From 2015 to 2017, he was a Post-Doctoral Research Fellow with the University of Technology Sydney, Sydney, where he is currently a Lecturer with the Global Big Data Technologies Centre. His current research interests include antennas and terahertz fibers.



**Y. Jay Guo** (F'14) received the bachelor's and master's degrees from Xidian University, Xi'an, China, in 1982 and 1984, respectively, and the Ph.D. degree from Xian Jiaotong University, Xi'an, in 1987.

He held various Senior Technology Leadership positions in Fujitsu, Siemens, and NEC, in U.K. He served as the Director of Commonwealth Scientific and Industrial Research Organization for over nine years, directing a number of ICT research portfolios. He is currently a Distinguished Professor and the founding Director of the Global Big Data Technologies Centre, University of Technology Sydney, Sydney, Australia. He has authored or co-authored over 400 research papers. He holds 24 patents in antennas and wireless systems. His current research interests include antennas, millimeter-wave and terahertz communications, sensing systems, and big data technologies.

Dr. Guo is a Fellow of the Australian Academy of Engineering and Technology, a Fellow of IET, and a member of the College of Experts of Australian Research Council. He was a recipient of the number of most prestigious Australian national awards. He was named one of the most Influential Engineers in Australia in 2014 and 2015. He has chaired numerous international conferences. He is the Chair Elect of International Steering Committee and International Symposium on Antennas and Propagation (ISAP). He was the International Advisory Committee Chair of the IEEE VTC2017, the General Chair of ISAP2015, iWAT2014, and WPMC'2014, and the TPC Chair of the 2010 IEEE WCNC, and 2012 and 2007 IEEE ISCIT. He served as a Guest Editor of special issues on *Antennas for Satellite Communications and Antennas and Propagation Aspects of 60–90 GHz Wireless Communications*, both in the IEEE TRANSACTIONS ON ANTENNAS AND PROPAGATION, special issue on *Communications Challenges and Dynamics for Unmanned Autonomous Vehicles*, the IEEE JOURNAL ON SELECTED AREAS IN COMMUNICATIONS, and special issue on *5G for Mission Critical Machine Communications, IEEE Network Magazine*.